NASDA report 03

Crystal growth of an InAs–GaAs binary semiconductor under terrestrial gravitational conditions

Toru Maekawa† and Takahiro Fukuda†

Satoshi Matsumoto††, Satoshi Adachi††,
Shinichi Yoda†† and Kyoichi Kinoshita††

† *Toyo University*
2100, Kujirai, Kawagoe, Saitama 350-8585, Japan
†† *National Space Development Agency of Japan*
2-1-1, Sengen, Tsukuba, Ibaraki 305-8505, Japan

We investigate the crystal growth process of an InAs-GaAs binary semiconductor by the Travelling Liquidus-Zone (TLZ) method under terrestrial gravitational conditions numerically and discuss the effect of the angle between the crystal growth direction and the gravity direction on the crystal growth process. First, we explain this new crystal growth technique and then develop a numerical model and calculation method of the growth of binary crystals, by which the flow field in the solution, the temperature and concentration fields in both the solution and crystals, and the shape and movement of the crystal–solution interfaces are determined. We focus, in particular, on the effect of the crystal size and the inclination angle on the crystal growth process. We find that (a) When the crystal size is 2 mm, convection is reduced and the concentration field is not seriously deformed as long as the inclination angle is less than 1 °. The degree of supercooling is remarkably reduced compared to the case when crystals are grown in the horizontal direction; (b) When the crystal size is greater than 5 mm, convection is intensified and the concentration field is seriously deformed. The degree of supercooling is increased as the inclination angle increases. The above results show that growing single crystals under terrestrial gravitational conditions are very difficult if the crystal size is greater than 5 mm.

1. Introduction

It is believed that convection induced in the melt or solution lowers the quality of grown crystals or causes polycrystallisation during the crystal growth process. Therefore, microgravity experiments of crystal growth have been carried out in recent years using drop towers, aircraft, rockets, space shuttles and satellites in order to reduce buoyancy convection and grow high quality crystals [1-7]. Now, the International Space Station is expected to come into operation in 2005 so that crystal growth experiments can be carried out under better conditions; that is, the long duration of low residual gravity conditions (~ 1 μg) is available.

Growing single crystals of uniform compositions of multi-component materials is very difficult compared to that of single-component materials since the shape and movement of the crystal–solution interfaces are determined by the concentration field in addition to the velocity and temperature fields. The interfacial temperature and concentration of the

solute vary along the crystal–solution interfaces. Note that the interfacial temperature is the melting temperature and therefore is constant along the interfaces in the case of single-component crystals. We have studied the growth process of an InAs-GaAs binary crystal numerically and found that it is very difficult to grow a crystal of uniform compositions by the Bridgman method even under 1 μg conditions because of the high Schmidt number, which is caused by the low diffusion coefficient of the solute [8]. Since the Prandtl number of semiconductor solutions is very low, the temperature field is not seriously deformed by convection, whereas the concentration field is very sensitive to convection and is deformed easily by it due to the high Schmidt number. As a result, the crystal interfaces are deformed as the crystal growth proceeds. There is another important factor, which makes the growth of multi-component crystals difficult; that is, supercooling induced in the solution during the crystal growth process. Even under microgravity conditions, supercooling occurs in the solution due to the high Schmidt number [9].

In this report, we focus on the growth of an $In_{0.3}Ga_{0.7}As$ crystal under 1g conditions from a macroscopic point of view based on continuum thermofluid dynamics coupled with first-order phase transition. We review the TLZ method briefly in Section 2. We introduce a numerical model of crystal growth by the TLZ method and explain the numerical procedure in Section 3. We show the result of the calculation and discuss the effect of the angle between the crystal growth and gravitational directions on the crystal growth process by the TLZ method. In the final section, we summarise the results obtained in this study.

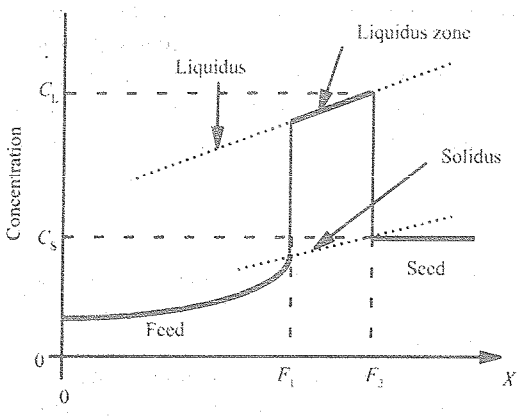

Fig.1 Travelling Liquidus-Zone method. A linear concentration distribution is established in the solution and crystal grows naturally following Eq.(1). Therefore, if the heater is moved at the spontaneous crystal growth rate, a crystal of uniform compositions can be grown.

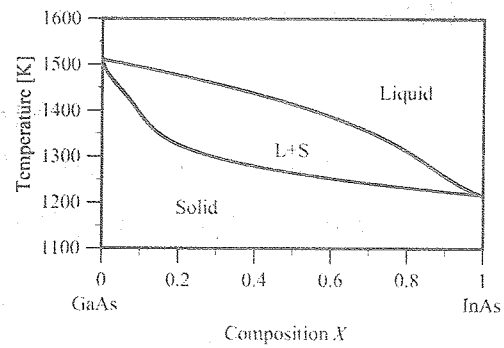

Fig.2 Pseudo-binary phase diagram of InAs-GaAs.

2. Travelling Liquidus-Zone method

As we mentioned, the concentration field and the crystal–solution interfaces are seriously deformed and an $In_{0.3}Ga_{0.7}As$ crystal of uniform compositions cannot be grown even under 1 μg conditions if $In_{0.3}Ga_{0.7}As$ crystals are grown by the Bridgman method due to the high Schmidt number. To improve this situation, Kinoshita *et al.* [11,12] proposed a new crystal growth method called the Travelling Liquidus-Zone (TLZ) method. We summarise the basic idea of crystal growth by the TLZ method in the following (see also Fig.1): A solution is sandwiched between the seed and feed crystals. The difference between the TLZ method and the ordinary zone melting method is that the temperature and solute concentration gradients are kept constant in the solution in the growth direction during the growth process in the case of the TLZ method (Fig.1), whereas the initial concentration is usually constant in the seed and feed crystals and the solution in the case of the zone melting method. If there is no convection, the linear temperature and concentration distributions can be maintained in the solution, and crystal grows spontaneously in the case of the TLZ method. The linear temperature and concentration distributions in the solution coincide very closely with the liquidus curve on the phase diagram if the temperature difference between the two interfaces is small (see Fig.2 for the phase diagram of the InAs-GaAs binary system [4].). That is why this crystal growth method is called the Travelling Liquidus-Zone method. However, supercooling always occurs in this case since the liquidus curve is, in fact, slightly convex (Fig.2). Therefore, reducing the degree of supercooling in the solution is very important in the

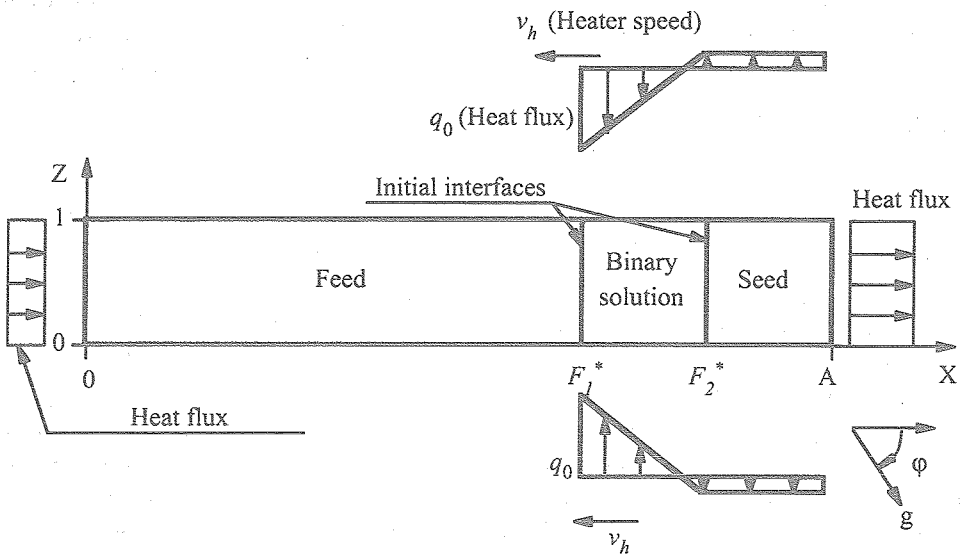

Fig.3 Outline of a crystal growth model of a binary InAs–GaAs semiconductor. A solution is sandwiched between seed and feed crystals. The inclination angle of gravity is φ. The velocity, temperature and concentration fields and the shape and movement of the interfaces are calculated numerically.

case of the TLZ method. The temperatures and solute concentrations at the crystal–solution interfaces and the movement of the interfaces are determined by the heat and mass balance at the interfaces and the liquidus and solidus curves. The growth rate can be estimated as follows in the case of one-dimensional diffusion limited growth by the TLZ method [11,12]:

$$v = \frac{D}{(c_S - c_L)} \left(\frac{\partial c}{\partial T}\right)_{Liquidus} \left(\frac{\partial T}{\partial x}\right). \quad (1)$$

where v is the growth rate of the seed crystal, D; the diffusion coefficient of the solute in the solvent, C_L; the saturation concentration of the solute at the solution side of the crystal–solution interface, C_S; the saturation concentration at the crystal side of the interface, $(\partial C/\partial T)_{Liquidus}$; the slope of the liquidus curve at the interfacial temperature, and $(\partial T/\partial x)$; the temperature gradient at the crystal–solution interface. The solute concentration decreases as crystal grows if the heater is not moved since the temperature at the seed crystal–solution interface rises with the movement of the interface. Therefore, if the heater is moved at the speed of the crystal growth rate v, the interfacial temperatures and concentrations can be kept constant at the crystal–solution interfaces during the crystal growth process. In other words, a crystal of uniform compositions can be grown. However, the temperature and concentration fields may be disturbed by convection. Therefore, we investigate the effect of convection on the crystal growth process by the TLZ method. We analyse the effect of the angle between the crystal growth direction and the gravitational direction on crystal growth. Note that when the angle is zero, that is, crystal grows in the antigravitational direction (see Fig.3), the system is rather thermally stable.

3. Numerical modelling and calculation method

In this section, we develop a numerical model of crystal growth by the TLZ method and introduce the governing equations of the growth of binary crystals. An outline of the numerical model of InAs–GaAs crystal growth is shown in Fig.3. The calculation area is divided into three regions: seed crystal, solution and feed crystal. The solution and the crystals are placed with an inclination angle φ and the heat flux is applied externally as shown in Fig.3, which is based on the heater of the crystal growth experimental system of the Japanese experimental module (JEM) in the International Space Station. The total amount of the heat input is equal to that of the heat output. The heaters move upwards so that the seed crystal grows in the $-x_1$ direction. The feed crystal–solution interface and the seed crystal–solution interface are, respectively, expressed by the following equations: $x_1 = F_1(x_2,t)$ and $x_1 = F_2(x_2,t)$. F_1 and F_2 are determined by the heat and mass balance at the interfaces and the liquidus and solidus curves on the phase diagram (see section 3.3).

The coordinate x_i, time t, pressure p, velocity u_i and temperature T are nondimensionalised as follows:

$$X_i \equiv \frac{x_i}{L}, \quad \tau \equiv \frac{t}{L^2/\nu_L}, \quad U_i \equiv \frac{u_i}{\nu_L/L},$$

$$P \equiv \frac{p}{\rho_0 \nu_L^2/L^2}, \quad \theta \equiv \frac{T - T_f}{q_0 L/\lambda_L}, \tag{2}$$

where L, ν, ρ_0, q_0 and λ are, respectively, the depth of the solution layer, the kinematic viscosity, the density, the maximum value of the heat flux (see Fig.3) and the thermal conductivity. Subscripts L, S and f represent liquid, solid and the melting point of InAs. Note that the concentration of InAs is already nondimensionalised (see Fig.2). The nondimensional governing equations are given in the following:

3.1 Governing equations in solution

The Boussinesq approximation being employed for the density change, the continuity equation, the momentum equation, the energy equation and the transport equation of the solute are introduced as follows:

Continuity equation:

$$\frac{\partial U_i}{\partial X_i} = 0 \tag{3}$$

Momentum equation:

$$\frac{\partial U_i}{\partial \tau} + U_j \frac{\partial U_i}{\partial X_j} = -\frac{\partial P}{\partial X_i} + \frac{\partial^2 U_i}{\partial X_j \partial X_j} + \frac{Ra^T}{Pr}\theta_L k_i - \frac{Ra^C}{Sc} C_L k_i, \tag{4}$$

where the buoyancy forces caused by both the temperature and concentration differences are taken into account and k_i is the unit vector in the antigravitational direction. In the case of the InAs–GaAs system, the density increases with a decrease in temperature and with an increase in the concentration of InAs.

Energy equation:

$$\frac{\partial \theta_L}{\partial \tau} + U_j \frac{\partial \theta_L}{\partial X_j} = \frac{1}{Pr} \frac{\partial^2 \theta_L}{\partial X_j \partial X_j}. \tag{5}$$

Transport equation of concentration of InAs:

$$\frac{\partial C_L}{\partial \tau} + U_j \frac{\partial C_L}{\partial X_j} = \frac{1}{Sc} \frac{\partial^2 C_L}{\partial X_j \partial X_j}. \tag{6}$$

We do not take into account the Sorét effect in this study since it has very little effect on the crystal growth process in the case of the InAs-GaAs system [8]. Ra^T, Ra^C, Pr and Sc are, respectively, the Rayleigh number based on the temperature difference, the Rayleigh number based on the concentration difference, the Prandtl number and the Schmidt number:

$$Ra^T \equiv \frac{\beta g q_0 L^4}{\lambda_L \kappa_L \nu_L}, \quad Ra^C \equiv \frac{\gamma g \Delta C L^3}{D_L \nu_L},$$

$$Pr \equiv \frac{\nu_L}{\kappa_L}, \quad Sc \equiv \frac{\nu_L}{D_L}, \tag{7}$$

where β, g, κ_L, γ and D_L are, respectively, the temperature coefficient of volume expansion, the gravitational acceleration, the thermal diffusivity, the concentration coefficient of volume expansion and the diffusion coefficient of the solute.

3.2 Governing equations in seed and feed crystals

The governing equations in the crystals are the heat conduction and diffusion equations.

Heat conduction equation:

$$\frac{\partial \theta_S}{\partial \tau} = \frac{K_{SL}}{Pr} \frac{\partial^2 \theta_S}{\partial X_j \partial X_j}. \tag{8}$$

Diffusion equation:

$$\frac{\partial C_S}{\partial \tau} = \frac{D_{SL}}{Sc} \frac{\partial^2 C_S}{\partial X_j \partial X_j}. \tag{9}$$

K_{SL} is the ratio of the thermal diffusivity of the crystal to that of the solution and D_{SL} is the ratio of the diffusion coefficient in the crystal to that in the solution:

$$K_{SL} \equiv \frac{\kappa_S}{\kappa_L}, \quad D_{SL} \equiv \frac{D_S}{D_L}. \tag{10}$$

3.3 Solution–crystal interfaces

The temperature and concentration at the crystal–solution interfaces and the positions of the interfaces are determined by the heat and mass balance at the interfaces and the liquidus and solidus curves on the phase diagram. The phase diagram of the InAs-GaAs binary system is shown in Fig.2.

Heat balance at the interfaces:

$$\frac{\partial F_i^*}{\partial \tau} = \frac{Sf}{Pr}\left\{\mp\left(\frac{\partial \theta_L}{\partial X_1} - \frac{\partial F_i^*}{\partial X_2}\frac{\partial \theta_L}{\partial X_2}\right) \pm G_{SL}\left(\frac{\partial \theta_S}{\partial X_1} - \frac{\partial F_i^*}{\partial X_2}\frac{\partial \theta_S}{\partial X_2}\right)\right\}. \tag{11}$$

Mass balance at the interfaces:

$$(C_L - C_S)\frac{\partial F_i^*}{\partial \tau} = \frac{1}{Sc}\left\{-\left(\frac{\partial C_L}{\partial X_1} - \frac{\partial F_i^*}{\partial X_2}\frac{\partial C_L}{\partial X_2}\right) + D_{SL}\left(\frac{\partial C_S}{\partial X_1} - \frac{\partial F_i^*}{\partial X_2}\frac{\partial C_S}{\partial X_2}\right)\right\}. \quad (12)$$

Here, F_i is the interfacial position nondimensionalised by L, and i (= 1, 2) corresponds to interfaces 1 and 2 (see Fig.3). Double signs, $\mp$ and $\pm$, correspond to i = 1 and 2. G_{SL} is the ratio of the thermal conductivity of the crystal to that of the solution, and Sf is the Stefan number:

$$G_{SL} \equiv \frac{\lambda_S}{\lambda_L}, \qquad Sf \equiv \frac{q_0 L}{\rho_0 L_{SL} \kappa_L}, \quad (13)$$

where L_{SL} is the latent heat per unit mass.

The temperature and concentration are not independent at the crystal–solution interfaces. The relations between the temperature and the concentration are given by the liquidus and solidus curves on the phase diagram. The temperature changes continuously at the interfaces; that is, $\theta_L = \theta_S$ at $X_1 = F_1^*$ and F_2^*, whereas concentration C_L is different from C_S at the interfaces. Since $\partial F_i^*/\partial \tau$ is common in Eqs.(11) and (12), the right-hand side of Eq.(11) is equal to the right-hand side of Eq.(12) divided by $(C_L - C_S)$. Therefore, the temperatures at the interfaces can be calculated. The interfacial temperatures having been determined, the concentrations at the interfaces are obtained via the liquidus and solidus curves and the positions of the interfaces F_i^* are calculated by Eq.(11). In this study, the relations between the concentrations and temperatures along the liquidus and solidus curves are approximated by polynomial functions of the fifth order. Here, we do not take into account the interfacial energy of the crystal–solution interfaces, that is, the Gibbs-Thompson effect [8,13], which has a crucial effect when the radius of the interfacial curvature is very small.

3.4 Numerical method and procedure

Since the crystal–solution interfaces move and the interfacial shapes change during the crystal growth process, we employ the boundary fit method to solve the governing equations efficiently [14]. The governing equations are transformed introducing the following new coordinates in the three regions:

Feed crystal:

$$\xi \equiv \frac{X_1}{F_1^*(X_2,\tau)}, \quad (14)$$

where F_1^* is the position of the feed crystal–solution interface (see Fig.3).

Solution:

$$\eta \equiv \frac{X_1 - F_1^*(X_2,\tau)}{F_2^*(X_2,\tau) - F_1^*(X_2,\tau)}, \quad (15)$$

where F_2^* is the position of the seed crystal–solution

Seed crystal:

$$\zeta \equiv \frac{X_1 - F_2^*(X_2,\tau)}{A - F_2^*(X_2,\tau)}, \quad (16)$$

where A is the aspect ratio of the system, that is, the ratio of the width of the whole system to the depth of the crystals and solution (Fig.3). The above coordinates are normalised as $0 \le \xi, \eta, \zeta \le 1$. The transformed governing equations are solved by the finite difference method. The time and spatial differentials are approximated by the first-order explicit formula and the second-order central formula, respectively.

Let us summarise the calculation procedure:

(1) The feed crystal–solution and seed crystal–solution interfaces are planar initially. The initial concentration of InAs in the seed crystal is 0.3, which is our target value, and that in the feed crystal is set at a constant value, which depends on the initial temperature gradient in the solution and the initial solution zone width. The concentrations at the solution sides of the interfaces are determined by the liquidus curve on the phase diagram. The concentration is linearly distributed in the solution and linear temperature distributions are given along the solution and crystals initially. Note that the temperatures at the interfaces are set at the equilibrium values corresponding to the interfacial concentrations.

(2) We start heating and cooling the system externally as shown in Fig.3. Note that the Rayleigh number is defined using q_0, which is the maximum value of the heat flux from the heater (see Fig.3).

(3) We solve the governing equations (3)-(6), (8) and (9) to obtain the velocity, temperature and concentration fields in the solution, and seed and feed crystals.

(4) The interfacial temperature and concentration are determined by the heat and mass balance equations and the liquidus and solidus curves on the phase diagram (see section 3.3).

(5) The interfacial temperature having been determined, the time derivatives of the

Table 1 Physical properties, system dimensions and growth conditions

Kinematic viscosity	ν_L	[$m^2 s^{-1}$]	1.5×10^{-7}
Density	ρ_0	[$kg\ m^{-3}$]	5.9×10^3
Thermal conductivity of solution	λ_L	[$W\ m^{-1} K^{-1}$]	3.0
Thermal conductivity of crystal	λ_S	[$W\ m^{-1} K^{-1}$]	1.2
Temperature coefficient of volume expansion	β	[K^{-1}]	9.34×10^{-5}
Concentration coefficient of volume expansion	γ	[--]	1.4×10^{-1}
Thermal diffusivity of solution	κ_L	[$m^2 s^{-1}$]	1.1×10^{-5}
Thermal diffusivity of crystal	κ_S	[$m^2 s^{-1}$]	3.0×10^{-6}
Diffusion coefficient of In in solution	D_L	[$m^2 s^{-1}$]	1.5×10^{-8}
Diffusion coefficient of In in crystal	D_S	[$m^2 s^{-1}$]	1.0×10^{-11}
Latent heat	L_{SL}	[$J\ kg^{-1}$]	5.0×10^5
Depth of solution and crystal	L	[mm]	2,5,10
Width of solution and crystal	W	[mm]	1.0
Heater speed	v_h	[$mm\ h^{-1}$]	0.4

crystal–solution interfaces are calculated by Eq.(11) and therefore the new positions of the interfaces are obtained. Using the new interfacial temperatures and concentrations and the new interfacial positions, procedures (3)-(5) are repeated.

The nondimensional parameters are estimated based on the physical properties of InAs and GaAs [15,16]. The crystal size, that is the width of the solution, is changed; 2 mm, 5 mm and 10 mm, and the height of the solution zone is fixed at 15 mm. The maximum heat flux, q_0, is 1.0 kW/m^2. The initial temperature gradient in the solution is 10 K/cm. The heater speed is set at 0.4 mm/h, which is the growth rates corresponding to the temperature gradients in the solution, that is, 10 K/cm, in the case of the one-dimensional diffusion limited crystal growth (see Eq.(1)). The physical properties, system dimensions and growth conditions are summarised in Table 1.

The governing equations were converted introducing the vorticity and stream function. The whole calculation space is divided by 123 × 31, 163 × 41 and 203 × 51 finite difference grids and the maximum differences in the stream function, temperature, concentration and positions of the interfaces caused by the differences in the number of the grid points were within 2 %. The results shown in the following section are based on the calculations using 163 × 41 grid points.

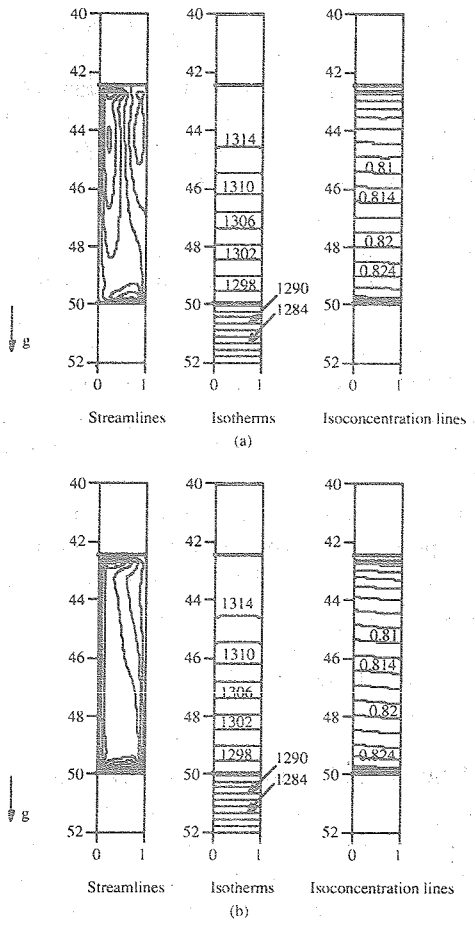

Fig.4 Streamlines, isotherms, isoconcentration lines and shapes of the crystal–solution interfaces. The crystal size is 2 mm. The initial solution zone height is 15 mm and the initial temperature gradient in the solution is 10 K/cm. 1 g is applied. $Ra^t = 1.16 \times 10^5$; $Ra^c = 7.62 \times 10^7$, $Sc = 10$, $Sf = 1.13 \times 10^{-2}$. (a) The inclination angle φ is 1°; (b) $\varphi = 5°$

4. Result and discussion

We investigate the effect of the angle between the crystal growth direction and the gravitational direction, and the crystal size on the crystal growth

process. Snapshots of the streamlines, isotherms, isoconcentration lines and the shapes of the interfaces are shown in Fig.4 for a crystal size of 2 mm. The initial solution zone height is 15 mm and the initial temperature gradient in the solution is 10 K/cm. Note that the scale is enlarged in the X-direction. When the inclination angle is 0.001°, almost symmetric vortices are generated and, as a result, the temperature and concentration fields are hardly deformed (Fig.4(a)), whereas as the angle increases, the flow patterns become asymmetric and the concentration field are deformed (Fig.4(b) and (c)). Note that the temperature field is not seriously deformed due to the low Prandtl number. The time variations of the maximum velocity induced in the solution are shown in Fig.5. As the angle increases, the maximum velocity increases and fluctuates in the early stage. The steady-state maximum velocity is of the order

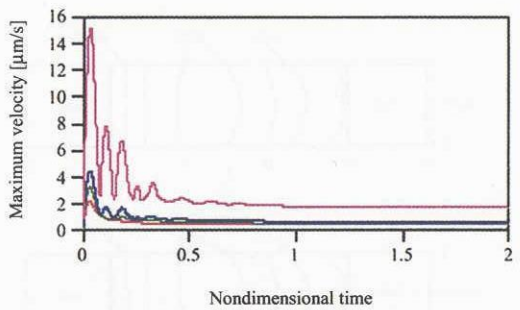

Fig.5 Time variations of maximum velocity in the solution. The crystal size is 2 mm. The initial solution zone height is 15 mm and the initial temperature gradient in the solution is 10 K/cm. 1 g is applied. ——: $\varphi = 0.001°$; ——: $\varphi = 0.5°$; ——: $\varphi = 1°$; ——: $\varphi = 5°$.

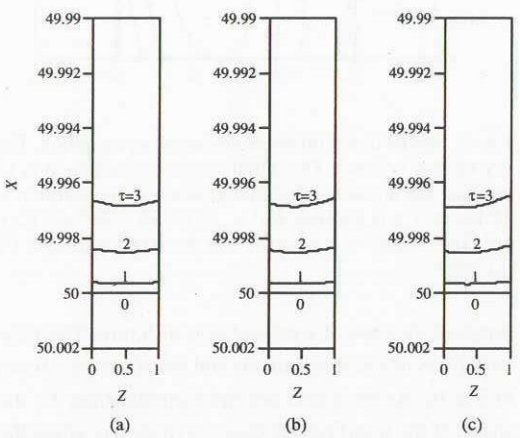

Fig.6 Time variations of the seed crystal–solution interface. The crystal size is 2 mm. The initial solution zone height is 15 mm and the initial temperature gradient in the solution is 10 K/cm. 1 g is applied. $Ra^T = 1.16 \times 10^{-2}$; $Ra^C = 7.62 \times 10^7$, $Sc = 10$, $Sf = 1.13 \times 10^{-2}$. (a) $\varphi = 0.001°$; (b) $\varphi = 1°$; (c) $\varphi = 2°$.

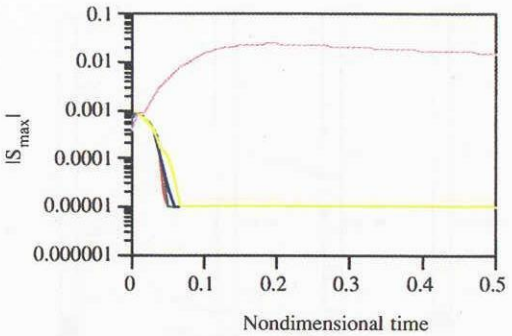

Fig.7 Time variations of the maximum value of the degree of supercooling. The crystal size is 2 mm. The initial solution zone height is 15 mm and the initial temperature gradient in the solution is 10 K/cm. 1 g is applied. ——: $\varphi = 0.001°$; ——: $\varphi = 1°$; ——: $\varphi = 2°$; ——: $\varphi = 5°$; ——: $\varphi = 90°$.

of μm/s in the case of a crystal size of 2 mm. The time variations of the solution–crystal interface are shown in Fig.6. As the angle increases, the shape of the interface becomes asymmetric even when the crystal size is 2 mm. Next, we check the effect of the inclination angle on the degree of supercooling induced in the solution. The degree of supercooling, S, is defined as follows:

$$S \equiv \frac{C_L - C_{L,sat}}{C_{L,sat}}, \tag{17}$$

where C_L is the local concentration in the solution and $C_{L,sat}$ is the saturation concentration corresponding to the local temperature (see the liquidus curve on the phase diagram (Fig.2).). The area where S is negative is supercooled. The time variations of the maximum values of the degree of supercooling, $|S|_{max}$, on the inclination angle are shown in Fig.7, where the size of crystal is 2 mm and the initial temperature gradient in the solution is 10 K/cm. The time variation of $|S|_{max}$ when crystal is grown in the horizontal direction is also shown in the figure. As is clearly seen, the degree of supercooling is reduced remarkably in the case of a crystal size of 2 mm if crystals are grown in antigravitational directions.

Snapshots of the streamlines, isotherms, isoconcentration lines and the shapes of the interfaces are shown in Fig.8 for a crystal size of 5 mm. The initial solution zone height is 15 mm and the initial temperature gradient in the solution is 10 K/cm. Even when the inclination angle is 0.001°, the convection pattern is already asymmetric (Fig.8(a)). The time variations of the maximum velocity induced in the solution are shown in Fig.9. As the angle increases, the maximum velocity increases. The steady-state maximum velocity is of the order of just less than

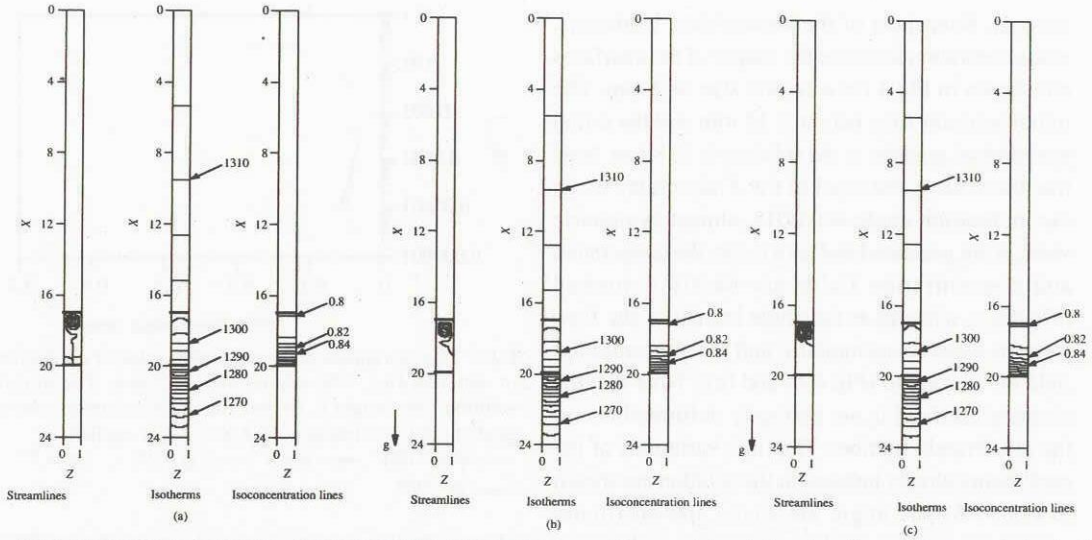

Fig.8 Streamlines, isotherms, isoconcentration lines and shapes of the crystal–solution interfaces. The crystal size is 5 mm. The initial solution zone height is 15 mm and the initial temperature gradient in the solution is 10 K/cm. 1 g is applied. $Ra^T = 1.16\times 10^{-2}$; $Ra^C = 7.62 \times 10^7$, $Sc = 10$, $Sf = 1.13 \times 10^{-2}$. (a) $\varphi = 0.001°$; (b) $\varphi = 1°$; (c) $\varphi = 5°$.

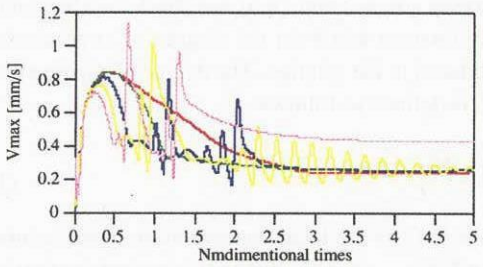

Fig.9 Time variations of maximum velocity in the solution. The crystal size is 5 mm. The initial solution zone height is 15 mm and the initial temperature gradient in the solution is 10 K/cm. 1 g is applied. —: $\varphi = 0.001°$; —: $\varphi = 0.1°$; —: $\varphi = 1°$; —: $\varphi = 2°$; —: $\varphi = 5°$.

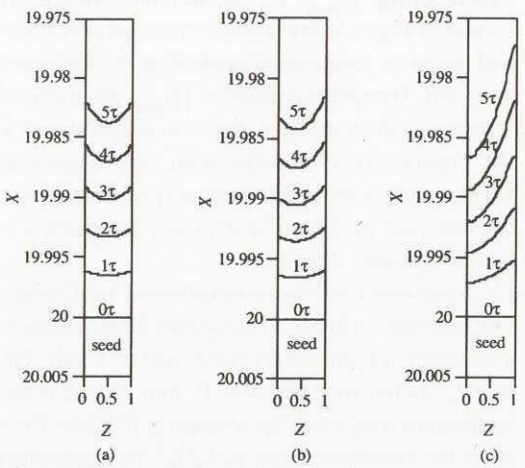

Fig.10 Time variations of the seed crystal–solution interface. The crystal size is 5 mm. The initial solution zone height is 15 mm and the initial temperature gradient in the solution is 10 K/cm. 1 g is applied. $Ra^T = 1.16\times 10^{-2}$; $Ra^C = 7.62 \times 10^7$, $Sc = 10$, $Sf = 1.13 \times 10^{-2}$. (a) $\varphi = 0.001°$; (b) $\varphi = 1°$; (c) $\varphi = 5°$.

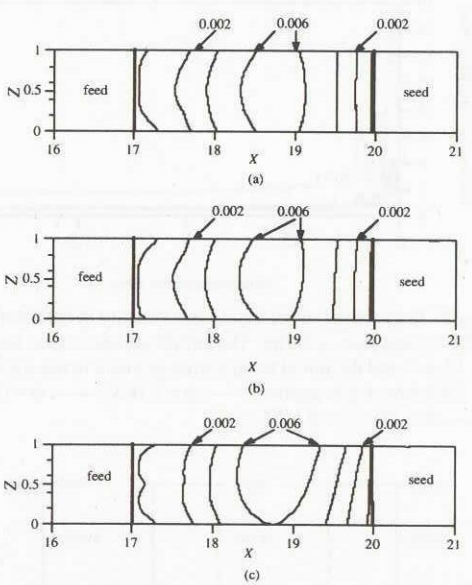

Fig.11 Spatial distributions of degree of supercooling. The crystal size is 5 mm. The initial solution zone height is 15 mm and the initial temperature gradient in the solution is 10 K/cm. 1 g is applied. $Ra^T = 1.16\times 10^{-2}$; $Ra^C = 7.62 \times 10^7$, $Sc = 10$, $Sf = 1.13 \times 10^{-2}$. (a) $\varphi = 0.001°$; (b) $\varphi = 1°$; (c) $\varphi = 5°$.

mm/s in the case of a crystal size of 5 mm. The time variations of the solution–crystal interface are shown in Fig.10. As the angle becomes greater than 1°, the shape of the interface becomes asymmetric when the crystal size is 5 mm. The spatial distributions of the degree of supercooling are shown in Fig.11, where the size of crystal is 5 mm and the initial temperature gradient in the solution is 10 K/cm. As the angle increases, the gradient of the degree of supercooling

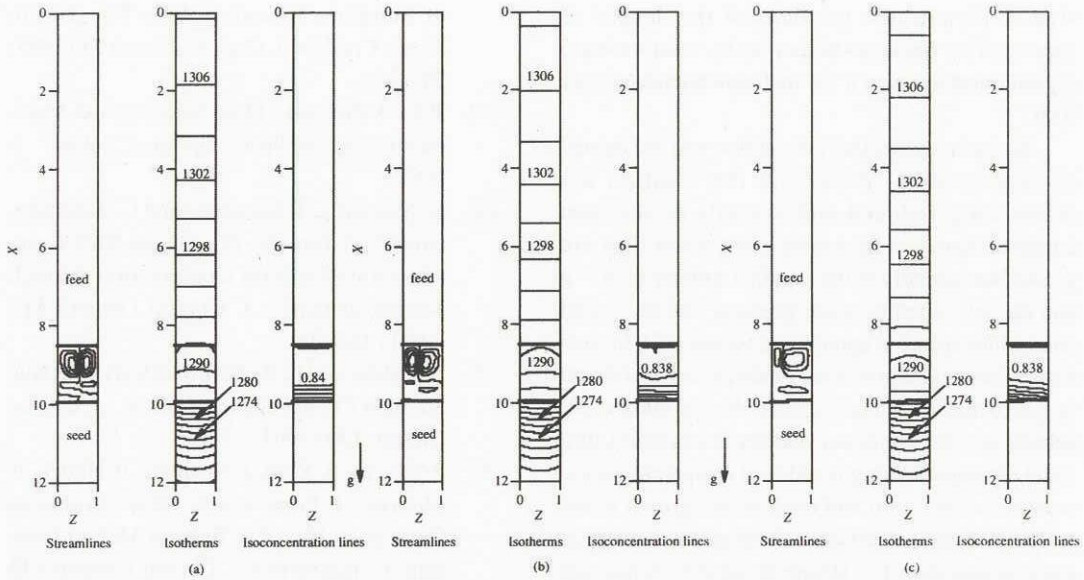

Fig.12 Streamlines, isotherms, isoconcentration lines and shapes of the crystal–solution interfaces. The crystal size is 10 mm. The initial solution zone height is 15 mm and the initial temperature gradient in the solution is 10 K/cm. 1 g is applied. $Ra^T = 1.16\times 10^{-2}$; $Ra^C = 7.62 \times 10^7$, $Sc = 10$, $Sf = 1.13 \times 10^{-2}$. (a) $\varphi = 0.001°$; (b) $\varphi = 1°$; (c) $\varphi = 5°$.

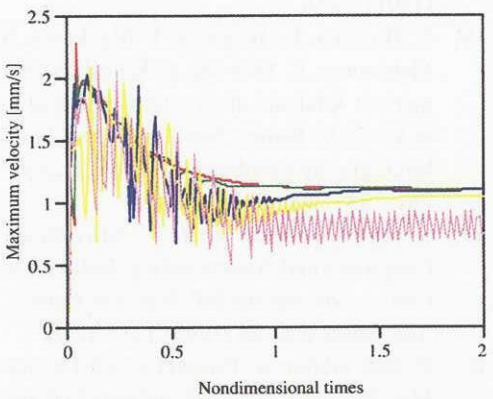

Fig.13 Time variations of maximum velocity in the solution. The crystal size is 10 mm. The initial solution zone height is 15 mm and the initial temperature gradient in the solution is 10 K/cm. 1 g is applied. —: $\varphi = 0.001°$; —: $\varphi = 0.1°$; —: $\varphi = 1°$; —: $\varphi = 2°$; —: $\varphi = 5°$.

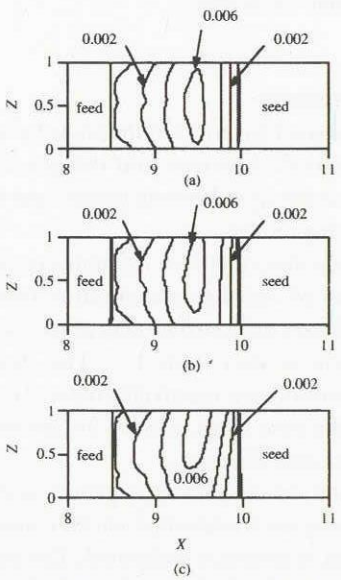

Fig.14 Spatial distributions of degree of supercooling. The crystal size is 10 mm. The initial solution zone height is 15 mm and the initial temperature gradient in the solution is 10 K/cm. 1 g is applied. $Ra^T = 1.16\times 10^{-2}$; $Ra^C = 7.62 \times 10^7$, $Sc = 10$, $Sf = 1.13 \times 10^{-2}$. (a) $\varphi = 0.001°$; (b) $\varphi = 1°$; (c) $\varphi = 5°$.

becomes higher at the top part (right-hand side) of the solution near the solution–seed crystal interface.

Finally, we show snapshots of the streamlines, isotherms, isoconcentration lines and the shapes of the interfaces in Fig.12 for a crystal size of 10 mm. The initial solution zone height is 15 mm and the initial temperature gradient in the solution is 10 K/cm. Even when the inclination angle is 0.001°, intensified convection is induced in the top part of the solution and, as a result, the concentration becomes uniform there and the steep concentration gradient is established at the solution–seed crystal interface (Fig.12(a)). As the inclination angle increases, convection is more intensified and the concentration field is greatly deformed (Figs.12 (b) and (c)). The time variations of the maximum velocity induced in the solution are shown in Fig.13. The velocity field fluctuates in the early stage and the order of the steady-state maximum velocity is 1 mm/s. The spatial distributions of the degree of supercooling are shown in Fig.14. When the crystal

size is 10 mm, the gradient of the degree of supercooling becomes higher at the solution–seed crystal interface even if the inclination angle is only 0.001 °.

We have shown that convection and the degree of supercooling induced in the solution are remarkably reduced and crystals of uniform compositions can be grown even when they are grown horizontally if the residual gravity is 10^{-6} g and the initial temperature gradient and the initial zone width are set at appropriate values [17]. In such a case, the maximum velocity induced in the solution is approximately 0.5 μm/s. According to our present calculation, the maximum velocity is less than 1 μm/s and the supercooling is reduced remarkably if the crystal size is 2 mm and crystals are grown in the antigravitational direction as long as the inclination angle is less than 1 °. However, as the crystal size increases, convection becomes more intensified and, as a result, single crystals of uniform compositions cannot be grown any more under terrestrial gravitational conditions.

5. Conclusions

We investigated the effect of the angle between the crystal growth direction and the gravitational direction on the crystal growth process and obtained the following results:

(a) When the crystal size is 2 mm, convection is reduced and the concentration field is not seriously deformed as long as the inclination angle is less than 1 °. The degree of supercooling is remarkably reduced compared to the case when crystals are grown in the horizontal direction.

(b) When the crystal size is greater than 5 mm, convection is intensified and the concentration field is seriously deformed. The degree of supercooling is increased as the inclination angle increases. The above results show that growing single crystals under terrestrial gravitational conditions are very difficult if the crystal size is greater than 5 mm.

References

[1] K. Kinoshita and K. Sugii, PbTe-SnTe Mutual Diffusion Coefficient at just above the $Pb_{0.8}Sn_{0.2}Te$ Solidus Temperature, J. Crystal Growth **67** (1984) 375-379.

[2] K. Kinoshita and K. Sugii, Bridgman Growth of Subgrain Boundary Free $Pb_{1-X}Sn_XTe$ Single Crystals, J. Crystal Growth **71** (1985) 283-288.

[3] H.U. Walter (ed), Fluid Sciences and Materials Science in Space, Springer, Tokyo, 1987.

[4] K. Nakajima, T. Kusunoki and C. Takenaka, Growth of Ternary $In_{1-X}Ga_XAs$ Bulk Crystals with a Uniform Composition through Supply of GaAs, J. Crystal Growth **113** (1991) 485-490.

[5] A. Baldus and K.W. Benz, Melt and Mettalic Solution Crystal Growth $CuInSe_2$, J. Crystal Growth **130** (1993) 37-44.

[6] P. Höschl, R. Grill, J. Svoboda, P. Hlídek, P. Moravec, J. Franc and E. Belas, Bridgman Growth of $Hg_{1-X}Cd_XTe$ from Melt of Constant Composition, J. Crystal Growth **138** (1994) 956-963.

[7] T. Kusunoki, C. Takenaka and K. Nakajima, LEC Growth of InGaAs Bulk Crystal Fed with a GaAs Source, J. Crystal Growth **112** (1991) 33-38.

[8] Y. Hiraoka, K. Ikegami, T. Maekawa, S. Matsumoto, S. Yoda and K. Kinoshita, Numerical Analysis of Crystal Growth of an InAs-GaAs Binary Semiconductor under Microgravity Conditions, J. Phys. D: Appl. Phys. **33** (2000) 2508-2518.

[9] S. Matsumoto and T. Maekawa, Constitutional Supercooling Induced by Convection during InP Solution Growth, Adv. Space Res. **24** (1999) 1215-1218.

[10] P. Bhattacharya, Properties of Lattice-Matched and Strained Indium Gallium Arsenide, INSPEC, London, 1993.

[11] K. Kinoshita, K. Kato, T. Tsuru, Y. Muramatsu and S. Yoda, Homogeneous $In_{0.3}Ga_{0.7}As$ Crystal growth by the Traveling Liquidus-Zone Method, J. Crystal Growth **225** (2001) 59-66.

[12] K. Kinoshita, Y. Hanaue, H. Nakamura, S. Yoda, M. Iwai, T. Tsuru and Y. Muramatsu, Growth of Homogeneous Mixed Crystals of $In_{0.3}Ga_{0.7}As$ by the Traveling Liquidus-Zone Method, J. Crystal Growth **237-239** (2002) 1859-1863.

[13] S.R. Coriell and G.B. McFadden, Morphological Stability Handbook of Crystal Growth vol.1b, ch.12, pp.785-857, North-Holland, Amsterdam, 1993.

[14] J.F. Thompson, Z.U.A. Warsi and C.W. Mastin, Numerical Grid Generation: Foun-

dations and Applications, Elsevier, New York, 1985.

[15] V.M. Glazov, S.N. Chizhevskaya and N.N. Glagoleva, Liquid Semiconductors, Plenum New York, 1969.

[16] K.H. Hellwege, Landolt-Börnstein: Numerical Data and Functional Relationships in Science and Technology vol.17, Springer, Berlin, 1982.

[17] T. Maekawa, Y. Sugiki, S. Matsumoto, S. Adachi, S. Yoda and K. Kinoshita, Numerical analysis of crystal growth of an InAs–GaAs binary semiconductor by the travelling liquidus-zone method under microgravity conditions, *Int. J. Heat Mass Transfer*, at press.